Influence of human cytomegalovirus glycoprotein O polymorphism on the inhibitory effect of soluble forms of trimer- and pentamer-specific entry receptors

Nadja Brait,[a] Tanja Stögerer,[a*] Julia Kalser,[a*] Barbara Adler,[b] Ines Kunz,[a] Max Benesch,[a] Barbara Kropff,[c] Michael Mach,[c] Elisabeth Puchhammer-Stöckl,[a] Irene Görzer,[a#]

[a]Center for Virology, Medical University of Vienna, Vienna, Austria

[b]Max von Pettenkofer-Institute for Virology, Ludwig-Maximilians-University Munich, Munich, Germany

[c]Virologisches Institut, Klinische und Molekulare Virologie, Friedrich-Alexander Universität Erlangen-Nürnberg, Erlangen, Germany

Running head: Glycoprotein O polymorphism and entry inhibitors

Address correspondence to Irene Görzer, irene.goerzer@meduniwien.ac.at.

* Present address:

Julia Kalser, Blood Service for Vienna, Lower Austria and Burgenland, Austrian Red Cross, Vienna, Austria

Tanja Stögerer, Institut National de la Recherche Scientifique, Centre Armand-Frappier Santé Biotechnologie, Laval, Canada

N.B. and T.S. contributed equally to this work

Word count abstract: 250

Word count importance: 142

Word count text: 6.144

Abstract

Human cytomegalovirus (HCMV) envelope glycoprotein complexes, gH/gL/gO-trimer and gH/gL/UL128L-pentamer, are important for cell-free HCMV entry. While soluble Nrp2-Fc (sNrp2-Fc) interferes with epithelial/endothelial cell entry through UL128, soluble PDGFRα-Fc (sPDGFRα-Fc) interacts with gO thereby inhibiting infection of all cell types. Since gO is the most variable subunit we investigated the influence of gO polymorphism on the inhibitory capacities of sPDGFRα-Fc and sNRP2-Fc.

Accordingly, gO genotype 1c (GT1c) sequence was fully or partially replaced by gO GT2b, GT3, GT5 sequences in TB40-BAC4-luc background. All mutants were tested for fibroblast and epithelial cell infectivity, for virions' gO and gH content, and for infection inhibition by sPDGFRα-Fc and sNrp2-Fc.

Full-length and partial gO GT swapping may strongly alter the virions' gO and gH levels associated with enhanced epithelial cell infectivity. All gO GT mutants except recombinant gO GT1c/3 displayed a near-complete inhibition at 1.25 µg/ml sPDGFRα-Fc on epithelial cells (98% versus 91%) and all on fibroblasts (≥ 99%). While gO GT replacement did not influence sNrp2-Fc inhibition at 1.25 µg/ml on epithelial cells (96%-98%), it rendered mutants with low gO levels moderately accessible to fibroblasts inhibition (20%-40%). In contrast to the steep sPDGFRα-Fc inhibition curves (slope >1.0), sNrp2-Fc dose-response curves on epithelial cells displayed slopes of ~1.0 suggesting functional differences between these entry inhibitors.

Our findings suggest that targeting of gO-trimer rather than UL128-pentamer might be a promising target to inhibit infectivity independent of the cell type, gO polymorphism, and gO/gH content. However, intragenic gO recombination may lead to moderate resistence to sPDGFRα-Fc inhibition.

53 **Importance**

54 Human cytomegalovirus (HCMV) is known for its broad cell tropism as reflected by the
55 different organs and tissues affected by HCMV infection. Hence, inhibition of HCMV entry
56 into distinct cell types could be considered as a promising therapeutic option to limit cell-free
57 HCMV infection. Soluble forms of cellular entry receptor PDGFRα rather than those of entry
58 receptor neuropilin-2 inhibit infection of multiple cell types. sPDGFRα specifically interacts
59 with gO of the trimeric gH/gL/gO envelope glycoprotein complex. HCMV strains may differ
60 with respect to the virions' amount of trimer and the highly polymorphic gO sequence. In this
61 study, we show that gO polymorphism rather than gO levels may affect the inhibitory capacity
62 of sPDGFRα. The finding that gO intragenic recombination may lead to moderate evasion from
63 sPDGFRα inhibition is of major value to the development of potential anti-HCMV therapeutic
64 compounds based on sPDGFRα.
65

Introduction

Human cytomegalovirus (HCMV) is a widely spread pathogen which may cause substantial harm in congenitally infected newborns and in patients undergoing severe immunosuppressive therapy (1). Natural HCMV transmission follows mainly through body fluids such as urine or saliva (2). Upon infection, HCMV is spread throughout the body infecting many of the major somatic cell types like fibroblasts, smooth muscle cells, endothelial cells, epithelial cells, neurons, and leukocytes (3).

Two virion envelope glycoprotein (gp) complexes of human cytomegalovirus, the trimer gH/gL/gO and the pentamer gH/gL/UL128-131, are known to play crucial roles in host cell entry (4-6). These two complexes share the same gH/gL heterodimer forming either with gO or with UL128 a disulfide bridge with gL-Cys144 (7). Cell-free virions which are infectious for multiple cell types rather than fibroblasts alone, thus resemble *in vivo* cell tropism, must harbour both gp complexes (8-10). HCMV strains show large differences in the relative levels of trimer and pentamer incorporated in their virions (11). It is suggested that the trimer–to-pentamer ratio influences the infection efficiency for the respective cell types (8, 12, 13) and that a number of HCMV genes have the capacity to impact the composition of the two gH/gL complexes (14).

Large sequence comparison analysis has shown that, among all subunits of the two gp complexes, glycoprotein O (gO) exhibits by far the highest sequence polymorphisms with up to 23% amino acid diversity among gO sequences (15-17). All known gO sequences cluster into 5 major groups which can further be divided into 8 genotypes (18, 19). A closer inspection of gO gene sequences in circulating HCMV strains revealed that recombination among distinct strains may have occurred at several positions along the gO gene (16, 17, 20-22), arguing that recombination may be an important driving force of gO sequence evolution. Although it appears that all 8 gO genotypes can form stable trimers (11), it is poorly understood what role gO polymorphism plays in cell tropism. As recently shown gO genotypes may influence the efficiency of epithelial cell infection through specific sequence characteristics (23) or via

affecting the relative levels of gH/gL complexes (11, 13). Moreover, it has recently been reported that the accessibility of certain gH or gH/gL epitopes for monoclonal antibodies differs among HCMV strains probably due to the distinct gO genotype sequences of the respective strains (24).

Over the last few years, a number of cellular interaction partners for both, the trimer and the pentamer have been identified (14). One of these cellular receptors, platelet-derived growth factor receptor alpha (PDGFRα), was identified to directly and specifically interact with gO parts of the trimer (25-27). This interaction enables entry of cell-free virions into fibroblasts, the only cell type which shows a high PDGFRα expression (28). Albeit, soluble forms of PDGFRα (sPDGFRα) can severely inhibit not only entry into fibroblasts, but also entry into endothelial and epithelial cells (25-27), and first observations indicate that the inhibitory capacity of sPDGFRα is effective against several HCMV strains even when they harbour a different gO genotype sequence (26).

Neuropilin-2 (NRP2), another recently identified host cell receptor for HCMV, specifically interacts with the UL128 subunit of the pentamer (29). This interaction is required for entry into endothelial and epithelial cells, most likely through endocytosis, but seems to be dispensable for entry into fibroblasts. Accordingly, a soluble form of NRP2 (sNRP2) inhibits endothelial and epithelial infection but not fibroblasts (29). Both PDGFRα and NRP2 likely function as the primary entry receptors for the trimer and pentamer, respectively, however, the modes of entry downstream of receptor binding may substantially differ. In particular, it appears that the trimer functions at steps which are required for entry into all cell types (14) which makes sPDGFRα or derivatives thereof a promising therapeutic tool against HCMV (30, 31).

In the present study, we now aimed to assess how gO polymorphism influences the inhibitory capacity of sPDGFRα and sNRP2, respectively. To this end, we generated a set of TB40-BAC4-luc-derived HCMV gO genotype mutant strains, five of them harbour one of the major gO genotype sequences and 2 of them carry a recombinant gO genotypic form. We showed that

subtle to moderate differences in the inhibitory capacities of the two entry inhibitors, sPDGFRα and sNRP2, are attributed to gO polymorphism.

Results

Cell-free infectivity of HCMV strains upon swapping of gO genotype sequences

In order to investigate the influence of gO polymorphisms on the cell entry inhibitors sPDGFRα and sNRP2, we generated a panel of gO genotype mutant viruses, in which the parental gO genotype sequence GT1c of TB40-BAC4-luc was fully or partially replaced by another gO GT sequence (see Figure 1, and Supplementary Figure 1). Correctness of the whole UL and US regions of fibroblast-derived reconstituted viruses were validated by whole genome sequencing. All experiments were done with reconstituted virus stocks without further passaging. For comparison analyses and comprehensiveness both the parental strain, referred to as gO GT1c, and the previously generated gO GT mutant, gO GT4 (23), were included in all experiments.

First, to assess the ability of the gO GT mutants to infect human foreskin fibroblasts (HFFs), cell-free virus stocks of gO GT1c and mutants were adjusted to a similar number of encapsidated genome equivalents (mean of 8.2 $\log_{10}$ copies/ml). Infectivity was quantified by monitoring luciferase expression in cell lysates 2 days post infection. Relative light units (RLUs) are the read out for the extent of infection. The $\log_{10}$ ratio of RLUs to encapsidated genomes was calculated and the fold change relative to gO GT1c was determined. Mutants and parental strain were incubated on the same plate to avoid inter-plate variability of RLU quantitation. As shown in Figure 2A, all gO GT mutants infected fibroblasts similarly efficient as gO GT1c.

Next, we determined the relative epithelial cell infectivity by simultaneously infecting both, epithelial cells and fibroblasts. Cell-free virus stocks were adjusted to achieve 300-1,500 RLUs in ARPE-19-infected cell lysates. Infection efficiencies were determined by luciferase assay 2 days post infection and the ratios of epithelial cell to fibroblast RLUs were calculated (see

Figure 2B). Mutant gO GT3 and the two recombinant forms, GT1c/GT3 and GT3/GT1c, along with gO GT4 displayed a significantly higher epithelial cell infectivity compared to gO GT1c. In summary, the data show that gO GT swapping, either full-length or partial, does not impair the capacity to infect fibroblasts but seems to affect epithelial cell tropism.

Content of gO and gH in the envelope of gO GT mutant viruses

Cell-free virions of parental strain TB40-BAC4-luc are characterized by high gO abundance and low UL128 expression. This is thought to result in a high trimer-to-pentamer ratio associated with a low efficiency for epithelial cell infection (12). Thus, we wanted to know whether the enhanced epithelial cell infectivity of gO GT3, gO GT1c/GT3 and gO GT3/GT1c results from changes in the trimer-to-pentamer ratio upon gO GT swapping. To this end, parental and mutant virions were purified from fibroblast supernatant and the amounts of gO and gH were determined by semi-quantitative western blot under reducing conditions. The total amount of virions was normalized to gB and/or major capsid protein (MCP). The gO content represents the amount of trimer and the gH level is assumed to indicate the overall amount of trimer and pentamer in virions. One representative immunoblot for each mutant is given in Figure 3, and the estimated virions' gO and gH contents are shown in Table 1. In comparison to gO GT1c the amount of virions' gO was severely reduced in gO GT3 (~ 80%), GT3/1c (~ 90%), GT1c/3 (~ 50%), a subtle reduction was found for gO GT5 (~ 30%), but no substantial changes for gO GT4 mutant virions. Notably, almost no gO was detectable in gO GT2b virions even when very high virion concentrations were used for immunoblotting (see Supplementary Figure 2). Although it cannot be excluded that gO GT2b virions harbour very low levels of gO it is more likely that the anti-gO antibody used in this study which is directed towards gO GT1c of TB40E (32) does not cross-react with gO GT2b while the gO genotypic forms GT3, GT4, and GT5 are well recognized (see Supplementary Figure 2). With regard to the gH content it appears that the mutant virions GT3 and GT1c/GT3 harbour 1.6 to 3.2 fold higher gH levels

whereas GT2b, GT4, and GT5 contain moderately lower levels as compared to gO GT1c. Hence, these data suggest a shift towards lower trimer-to-pentamer ratio upon full-length and partial swapping of GT3 sequences but not upon replacement of GT1c by GT4 and GT5 sequences.

Inhibition of cell-free fibroblast and epithelial cell infectivity by soluble PDGFRα-Fc

Since all gO GT mutants retained the ability to infect fibroblasts and epithelial cells, we were able to directly compare the inhibitory capacity of sPDGFRα-Fc between the five major gO genotypic and the two recombinant forms. The inhibition experiments were performed with a fixed amount of infectious viruses pre-incubated for 2 hours with a 2-fold dilution series of sPDGFRα-Fc ranging from 0.0025 to 0.625 µg/ml. After another 2 hour-incubation on fibroblasts or epithelial cells, respectively, cells were washed and subsequently incubated with fresh medium for further 2 days. RLUs were monitored by a luciferase assay and plotted against the concentration of sPDGFRα-Fc.

First, the appropriate amount of infectious input virus was determined using three different virus dilutions of parental strain gO GT1c. As shown in Figure 4A and 4B there was no substantial change in the overall shape of the dose-dependent inhibition over a wide range of input infectivity. Thus, for all further inhibition experiments the cell-free virus stocks were normalized to similar RLUs within the tested range (see Materials and Methods). In all mutants, cell-free infectivity was inhibited by sPDGFRα-Fc in a dose-dependent manner. One representative curve for gO GT1c and the gO GT mutants is shown in Figure 4C and 4D. The half-maximal inhibition (IC_{50}) as calculated by non-linear regression ranged from 49 ng/ml to 73 ng/ml for fibroblasts and from 24 ng/ml to 56 ng/ml for epithelial cells (see Table 2). None of the mutants' IC_{50} value significantly differed from IC_{50} of parental strain. Moreover, there was no difference between parental strain and mutants in the overall steep shape of the dose-response curves (slopes >1), neither in fibroblasts nor in epithelial cells, except for one of the

196 recombinant mutants, gO GT1c/3, in epithelial cells. This gO mutant showed a shallower dose-
197 response curve with a slope of 1.0 to 2.6 (see Table 2). The slope parameter mathematically
198 analogous to the Hill coefficient is a measure of cooperativity (33) in the binding of multiple
199 ligands (e.g. sPDGFRα-Fc) to linked binding sites (e.g. gO). Dose-response curves with a slope
200 of about 1.0 are indicative for non-cooperativity which means the ligand binds at each site
201 independently. In contrast, steep curves with slopes much larger than 1.0 are thought to result
202 from a form of positive cooperative effects upon ligand binding (33). Hence, these findings
203 suggest that the presumed positive cooperativity is weakened when sPDGFRα-Fc binds to gO
204 GT1c/3.
205 Next, we determined the maximal extent of inhibition at 1.25 µg/ml sPDGFRα-Fc calculated
206 as 1 – (RLU after pretreatment / RLU of untreated virus stocks). The inhibition of fibroblast
207 infectivity was almost complete (> 99%) and did not differ between gO GT1c and mutants (see
208 Figure 4E). In epithelial cells, in contrast, one of the recombinant mutants, gO GT1c/3, retained
209 a significantly higher infectivity (mean: 9%) at this inhibitor concentration compared to gO
210 GT1c. The other mutants did not differ from the parental strain. The reduced epithelial cell
211 inhibition of gO GT1c/3 by sPDGFRα-Fc is well in accordance with the shallower shape of the
212 dose-response curve (Figure 4D). Notably, the inhibition efficiency was slightly less effective
213 in epithelial cells (~ 98 – 99%) than in fibroblasts for gO GT1c and the mutants, GT2b, GT3,
214 and GT3/1c (see Figure 4E).
215 In summary, these findings show that not only the five major genotypic forms of gO are
216 recognized by sPDGFRα-Fc but also recombinant forms of gO. Albeit, one recombinant version
217 of gO seems to be less effectively inhibited by sPDGFRα-Fc on epithelial cells.
218
219 **Inhibition of cell-free fibroblast and epithelial cell infectivity by soluble NRP2-Fc**
220 It has recently been reported that soluble forms of NRP2 which specifically bind to UL128,
221 inhibit epithelial cell infection while fibroblast infection remains largely unaffected (29). We

222 wanted to know whether alterations in the virions' gO and gH content upon gO GT swapping
223 may indirectly affect the inhibitory capacity of sNRP2-Fc. To address this question, first we
224 performed inhibition experiments on epithelial cells using a 2-fold dilution series of sNRP2-Fc
225 (range: 0.0025 to 0.626 µg/ml) and a fixed amount of RLU-normalized gO GT virions as
226 described for sPDGFRα-Fc. Two independent experiments were performed for each mutant
227 along with the parental strain and one representative curve is shown in Figure 5A. The dose-
228 dependent inhibition was similar between parental strain and gO GT mutants, the dose-response
229 curves displayed slopes of about 1.0 (range: 0.7 to 2.1) and the IC_{50} values ranged from 31 to
230 90 ng/ml (see Table 2). These findings indicate that neither the gO genotypic form nor changes
231 in the virion's gO content influences the capacity of sNRP2-Fc for epithelial cell inhibition.
232 Finally, we wanted to assess the maximum inhibitory capacity of 1.25 µg/ml sNRP2-Fc on
233 epithelial cells and whether such high inhibitor concentrations also have an effect on fibroblast
234 infectivity. As shown in Figure 5B, epithelial cell infectivity was 96% to 98% reduced in all
235 mutant viruses and this did not significantly differ between parental strain and mutants.
236 Interestingly, although the fibroblast infectivity was almost unaffected in parental strain and in
237 two of the mutants, GT2b and GT5, a moderate reduction in fibroblast infectivity of 20% to
238 40% was observed for the other mutants and this reached statistical significance for the
239 recombinant mutant gO GT1c/3. From these data it appears that gO differences upon GT
240 swapping may render mutant virions partially accessible to sNRP2-Fc inhibition on fibroblasts.
241
242 **Discussion**
243 The two envelope glycoprotein complexes, gH/gL/gO-trimer and gH/gL/UL128L-pentamer,
244 which share the same gH/gL heterodimer, play major roles in HCMV cell entry. In the present
245 study, we focussed on gO, the critical subunit of the trimer. A special hallmark of gO is its high
246 polymorphism with an overall amino acid diversity of ~ 20% (18, 19). To learn more about
247 potential functional differences attributed to gO polymorphism, we fully or partially swapped

gO gene sequences in the otherwise identical TB40-BAC4-luc background, tested the set of gO mutants for their capability to infect fibroblasts and epithelial cells, for their relative composition of gO and gH in cell-free virions, and evaluated the inhibitory capacity of sPDGFRα-Fc in comparison to sNRP2 inhibition.

First, we demonstrate that gO GT swapping, either partial or full-length, does not substantially affect fibroblast infectivity but may lead to an increase in relative epithelial cell infectivity. In particular, the mutants gO GT3, GT3/1c, and GT1c/3, which displayed the strongest enhancement in epithelial cell infection, contained substantially lower gO but higher gH levels in their cell-free virions as compared to parental strain. Previous studies have revealed that gO and UL128 compete for binding to the same gL cysteine residue in gH/gL (7) which in turn regulates the trimer to pentamer ratio (7, 8) and this renders virions more infectious for fibroblasts (high trimer to pentamer ratio) or epithelial cells (low trimer to pentamer ratio) (11, 12). Since parental strain TB40-BAC4-luc is characterized by vastly more gO than UL128 accompanied by a low epithelial cell infectivity (12) it is likely that the opposite changes in gO and gH levels upon partial or full-length GT3 swapping cause a shift towards lower trimer to pentamer ratio which may well explain the increase in epithelial cell infectivity. The impact of the relative composition of gO and gH in terms of epithelial cell infectivity is further underlined by the observation that replacement of gO GT1c by GT5 which causes a subtle reduction in both, gO and gH, has no effect on epithelial cell infectivity. Similarly as recently reported, gO GT1b to GT5 swapping and vice versa has also no effect on gO expression levels (13). Together, these findings suggest that the relative abundance of gO and gH incorporated into cell-free virions is influenced by the gO genotypic form. Recently, UL148 has been identified to regulate the trimer to pentamer ratio by stabilizing gO within the endoplasmatic reticulum (34, 35). It is tempting to speculate that the regulatory capability of UL148 is influenced by the gO sequence. Additionally, it cannot be excluded that GT sequence-specific characteristics directly modify the capacity of cell-free virions for entry into epithelial cells, since gO GT4

displayed an enhanced epithelial cell tropism without substantial alterations in gO and gH abundance, as previously shown (23).

Remarkably, despite significant differences in epithelial cell tropism, the fibroblast infectivity was similar among the mutants and parental strain. These findings indicate that neither changes in gO and gH abundance nor gO GT sequence-specific characteristics affect the capacity for fibroblast infection. Moreover, these data lead to the conclusion that all of these gO genotypic forms can bind to the cellular fibroblast receptor PDGFRα with similar efficiency. Strikingly, a minimum level of gO on cell-free virions seems to be still sufficient for normal fibroblast infection under the tested *in vitro* conditions as in particular gO GT3 and gO GT1c/3 mutants display very low gO levels. Taken together, these observations provide clear evidence that gO polymorphism has a substantial impact on epithelial cell but not on fibroblast infectivity. Further investigations will clarify how differences in the gO and gH abundance and/or GT-specific sequence characteristics affect epithelial cell entry of cell-free virions.

Recombination among different HCMV strains appears to be a major driving force in HCMV evolution as shown by numerous studies (36). Recently, the recombination density throughout the genome was deeply investigated by whole genome sequence comparisons exploring past and recent recombination events as well (16, 20, 21). A particularly interesting finding was the identification of pervasive genome-wide recombination generating diversity both within and between genes (16, 21). So far, little is known about potential functional consequences for individual genes upon intragenic recombination. In the present study, we have now included two chimeric gO GT mutants, each of them carrying a recombinant gO genotypic form composed of GT1c and GT3 sequences. One of them, gO GT3/1c, harbours the recombination breakpoint within the conserved C-terminal part of gO and this mutant differs from full-length gO GT3 in only 4 amino acid residues. The recombination breakpoint of the other one, gO GT1c/3, is located in a small identical sequence stretch between GT1c and GT3 in the otherwise highly polymorphic N-terminal part of gO. Recombination resulted in a severely altered gO

sequence with an amino acid diversity of 9% from GT1c and of 10% from GT3. Strikingly, both recombinant gO mutants not only fully retained the ability to infect fibroblasts they even displayed an enhancement in epithelial cell infectivity comparable to full-length GT3 mutant. As discussed above, the change in gO and gH abundance may cause the observed epithelial cell phenotype. Accordingly, these findings indicate that recombination within the gO gene could be considered as an important function for HCMV to generate (i) gene diversity with or without modified functions and (ii) novel combinations of neighbouring loci even when they are highly diverse. This is well in concordance with previously reported sequencing data showing that recombination within gO may sporadically occur also *in vivo* despite a strong linkage between gO and the adjacent, partly overlapping gN gene (16, 17, 21, 22, 37).

Recent studies have shown that PDGFRα specifically interacts with the gO subunit of the trimer which is required for entry into fibroblasts (25-28). As soluble forms of PDGFRα or derivatives thereof can inhibit cell-free infection of several cell types (26) it appears that binding of sPDGFRα to gO interferes with trimer-mediated function(s) widely required for cell entry. We now demonstrate that representatives of the five major gO genotypic forms, GT1c, GT2b, GT3, GT4, and GT5, are similarly recognized by sPDGFRα and upon pretreatment with sPDGFRα-Fc both, fibroblast and epithelial cell infectivity was strongly inhibited. These data are well in line with previous reports showing the inhibitory capacity of sPDGFRα for several distinct HCMV strains (26). Notably, even at a concentration of 1.25µg/ml sPDGFRα we observed a residual infectivity of about 1 - 2% in epithelial cells, while in fibroblasts the inhibition was almost complete (≥ 99%) similar as shown previously (27). Thus, it is tempting to speculate that a trimer-independent entry mechanism accounts for the residual infectivity. Alternatively, it is also possible that not all virions are neutralized at this concentration allowing for a residual infection.

Remarkably, one of the two recombinant mutants, gO GT1c/GT3, displayed a significantly lower sensitivity for sPDGFRα inhibition on epithelial cells than the other mutants while the

fibroblast inhibition was similarly effective. As mentioned above this mutant comprises its recombination site in the highly polymorphic N-terminal region of the protein, which only recently was suggested to contain the PDGFRα receptor binding domain (31). By mutational analysis the authors identified a small stretch from amino acid 117 to 121 causing the strongest impairment of sPDGFRα binding to virus particles and consequently also a reduced virus penetration into fibroblasts. Although this peptide site overlaps with the recombination site of GT1c/GT3, the specific sequence remained unchanged upon recombination suggesting that sPDGFRα binding to this recombinant form of gO is not impaired. This presumption fits well to the finding that gO GT1c/GT3 mutant does not display a phenotype in fibroblast infectivity while mutants with a mutation in this particular peptide sequence showed reduced penetration into fibroblasts (31). Hence, we assume that the impaired sPDGFRα inhibition for gO GT1c/GT3 mutant on epithelial cells is not caused by a lower binding of sPDGFRα to gO but rather by an impaired interference with a downstream entry step mediated by the trimer.

The assumption that binding of sPDGFRα to gO-trimer affects more entry properties than the unique block of the receptor binding site is further strengthened by our findings that inhibition with 2-fold serial dilutions of sPDGFRα led to steep dose-response curves in both fibroblasts and epithelial cells. Such steep inhibition curves with a slope of much greater than 1 are thought to result from a form of positive cooperative effects upon ligand binding (33). Remarkably, the steepness of the sPDGFRα-Fc dose-inhibition curves were not affected by the gO content in virions, nor by the amount of input virions. The underlying mechanisms are not yet clearly understood but following scenarios may explain why sPDGFRα-bound virions become rapidly inactive for cell entry: binding of sPDGFRα to virions leads to (i) steric hindrance and/or conformational changes of the gO-trimer which affects multiple sPDGFRα binding sites on the virion, (ii) cluster formation of trimers and/or other envelope complexes which causes that multiple gO binding sites on the virion are rapidly blocked, (iii) changes of gB prefusion into gB postfusion conformation (under the assumption that the trimer stabilizes the gB prefusion

conformation) which renders virions inactive for entry, and/or (iv) cluster formation of multiple virions. Although these proposed scenarios await further clarification, from our data it becomes clear that a presumed cooperative effect triggered by sPDGFRα does not differ among the five major gO genotypes.

When we compared the dose-response curves of sPDGFRα with those of sNRP2, a recently identified entry inhibitor for epithelial cells (29), it becomes obvious that the mechanisms of action substantially differ between these two entry inhibitors. The dose-response curves of sNRP2 displayed a slope of about 1 – 2 meaning that binding of sNRP2 to its interaction partner UL128 of the pentamer causes no further effects beside the block of the binding site. There was also seen no difference among the gO GT mutants and parental strain indicating that neither gO abundance nor gO GT-specific characteristics influence the binding efficiency of sNRP2. Notably, all gO mutants along with parental strain displayed a residual epithelial cell infectivity of about 2-3% at a concentration of 1.25 µg/ml sNRP2. Whether an NRP2-independent entry pathway circumvents a complete inhibition or whether not all virions are neutralized by this concentration of sNRP2 yet awaits further investigation. As recently reported, fibroblast infection is largely unaffected by sNRP2 (29). In overall, this finding is well in concordance with our data. However, we observed a subtle inhibition of fibroblast infectivity by high concentrations of sNRP2 in those mutant virions which displayed very low amounts of gO. Thus, it is presumable that binding of high amounts of sNRP2 to virions lead to steric hindrance of the trimer which becomes visible only for virions with low gO levels.

In conclusion, in this study we show that the trimer to pentamer ratio which is substantially affected by gO polymorphism has no influence on the inhibitory capacity of sPDGFRα but may render virions slightly susceptible to sNRP2 inhibition on fibroblasts. When sPDGFRα or derivates thereof are considered for a therapeutic option to HCMV infection it should be taken into account that gO intragenic recombination may lead to partial evasion from sPDGFRα inhibition.

Material and Methods

Cells

Human foreskin fibroblasts (HFFs) were cultured in minimum essential medium Eagle (MEM; Sigma-Aldrich, St. Louis, Missouri) supplemented with 10% heat-inactivated fetal bovine serum (FBS; Capricorn Scientific, Ebsdorfergrund, Germany) and 0.5% neomycin (Sigma-Aldrich). Human adult retinal pigmented epithelial cells (ARPE-19; ATCC, Manassas, Virginia) were cultured in Dulbecco's modified Eagle medium/nutrient mixture F12 (PAN-Biotech, Aidenbach, Germany) supplemented with 10% FBS and 1% penicillin-streptomycin (Thermo Fisher) or in MEM supplemented with 10% FBS and 0.5% neomycin.

Generation of gO mutant BAC clones by en passant mutagenesis

All HCMV gO mutant strains were derived from the bacterial artificial chromosome (BAC) clone TB40-BAC4-luc (38). By "en passant" mutagenesis in *E.coli* GS1783 (39), the gO GT1c sequence of TB40-BAC4-luc was fully exchanged by GT2b, GT3, and GT5 respectively, and partially by gO GT3, either at the 5' or 3' end of gO GT1c ORF. For generation of full-length gO BAC mutants, a gO deletion mutant was used in which the whole gO ORF sequence was deleted. This ensured recombination between transfer plasmid and BAC-DNA solely upstream and downstream of the gO ORF sequence. For generation of recombinant BAC mutants, GT3/1c and GT1c/3, original TB40-BAC4-luc BAC DNA was used and both chimeric versions resulted from recombination within the gO GT1c ORF. First, a set of recombination cassettes were generated and the primer pairs used are listed in Supplementary table 1. For this, inserts containing a kanamycin resistance gene, flanked on one side by an 18-bp I-Sce I restriction sequence and a gO GT-specific 50-bp sequence, and on both sides by a Sac I or Nde I restriction site, respectively, were generated by PCR using pEP-Kan-S (kindly provided by Nikolaus Osterrieder). Second, each individual insert was cloned into the corresponding restriction site of gO GT sequence carried by pEX-A258 ordered from Eurofins Genomics (Luxembourg). The

404 resulting transfer plasmids were used as template to generate the PCR-derived recombination
405 cassettes containing extensions of ~50 bp sequences on each end for homologous
406 recombination. The recombination cassettes were electroporated into recombination-competent
407 *E.coli* GS1783 carrying the full-length or gO-deleted TB40-BAC4-luc DNA. After
408 electroporation, recombination-positive *E.colis* were subjected to kanamycin selection, and the
409 introduced non-HCMV sequences were removed within *E.coli* by cleavage at the I-Sce I site
410 and a second red recombination. Positive kanamycin-sensitive, chloramphenicol-resistant
411 bacteria colonies were selected. Finally, recombinant BAC DNAs were isolated from positive
412 clones and the correctness of the BAC DNA sequence was verified by whole genome
413 sequencing (see below). Further, overnight *E.coli* cultures of positive clones were stored at -80
414 °C until further use.
415
416 **BAC-derived gO mutant HCMV strains**
417 Infectious viruses were generated by reconstitution as described previously (23). Briefly,
418 mutant BAC DNAs were purified from *E.coli* using the Nucleobond BAC100 kit (Macherey-
419 Nagel, Düren, Germany). The day before transfection, HFFs were seeded in 6-well plates (3 x
420 10^5 cells/well) and then 2 µg of BAC DNA, 1 µg of pCMV71 DNA (plasmid was kindly
421 provided by Mark Stinski, University of Iowa) and 9 µl of ViaFect reagent (Promega, Madison,
422 Wisconsin) were mixed together with 100 µl of MEM without antibiotics, incubated for 15 min
423 at room temperature and then added to the cells. 24 h after transfection, cells were washed with
424 PBS and fresh MEM with antibiotics was added. One week after transfection, cells were
425 trypsinized and transferred into 25 cm^2 cell culture flasks. When CPE was 90-100%,
426 supernatants were cleared by centrifugation at 4°C for 20 min at 4,000 x *g* and stored as cell-
427 free viral stocks in aliquots at -80 °C. For infection and inhibition analyses, all aliquots were
428 used only once to avoid multiple freeze-thaw cycles. Furthermore, one aliquot per reconstitution
429 was subjected (i) to next generation sequencing to confirm the correctness of the complete UL

and US genomic regions, (ii) to DNase treatment to assess the amount of encapsidated genomes, and (iii) to RLU measurements in order to normalize virus stocks in subsequent experiments. Two independent reconstitutions were performed for each mutant.

Whole genome sequencing

DNA from BAC purification (as described above) and extracted DNA from DNase-treated or untreated viral stocks from HFF cell culture supernatants upon reconstitution were quantified using the Qubit 2.0 fluorometer (Thermo Fisher) according to the manufacturer's instructions. One to two ng of DNA per sample were taken for library preparation using the Nextera XT DNA Library Preparation Kit and uniquely indexed samples using the Nextera XT Index Kit were pooled and sequenced together (both Illumina, San Diego, California). Pooled libraries were sequenced with paired-end reads (2x150-250) on a MiSeq system using v2 or v3 sequencing reaction chemistry (Illumina). Data were analyzed by CLC genomics workbench v12 software (Qiagen). Low-quality reads were trimmed and in average 52 - 80% of reads mapped to the reference genome.

Determination of encapsidated HCMV genomes in virus stocks

In order to remove non-encapsidated viral DNA and free cellular DNA, fibroblast-derived virus stocks were treated with TurboDNase (Thermo Fisher). For this, 100 µl of master mix (73 µl H_2O, 20 µl 10x DNase buffer, 5 µl 10x PBS, 2 µl TurboDNase (2 u/µl)) were added to 100 µl of sample and incubated for 1 h at 37°C in a thermoshaker at 1,400 rpm. Immediately thereafter, the total reaction volume was added to 2ml lysis buffer and DNA was extracted using the bead-based NucliSens EasyMag extractor (BioMérieux, Marcy-l'Étoile, France) according to the manufacturer's protocol. DNA was eluted in 50 µl of nuclease-free H_2O.

HCMV-specific quantitative PCR

456 HCMV-DNA was quantitated using an in-house real-time qPCR amplifying a conserved region
457 within US17 (forward primer GCGTGCTTTTTAGCCTCTGCA (10 pM), the reverse primer
458 AAAAGTTTGTGCCCCAACGGTA (10 pM), TaqMan probe FAM-TGATCGGCGTTATCG
459 CGTTCTTGATC-TAMRA (2 pM)) as previously described (23).
460
461 **Normalization of parental and mutant virus stocks**
462 The firefly luciferase gene of HCMV strain TB40-BAC4-luc allows to monitor relative light
463 units (RLUs) in infected cell lysates as a read out for infection efficiency (40). For
464 normalization of parental strain and mutant virus stocks to similar RLUs, HFFs and ARPE-19
465 cells were seeded in white, clear, flat-bottom 96-well plates (Corning, Corning, New York) at
466 a density of 1 x 10^4 cells/well. The following day, viral stocks were serially 2-fold diluted in
467 cell culture medium and 100 µl of viral dilution per well were used to infect the cells in
468 triplicates for 2 h at 37 °C. Cells were washed three times with PBS, supplied with 100 µl of
469 medium and incubated further at 37 °C for 2 days. RLUs were determined by luciferase assay
470 of cell lysates according to the manufacturer's protocol (SteadyGlo Luciferase Assay System,
471 Promega) and measured in a Victor Light 1420 plate reader (PerkinElmer, Waltham,
472 Massachusetts). Mean RLUs of triplicates were calculated for normalization. For inhibition
473 assays viral stock dilutions generating 1,000 to 20,000 RLUs for both, HFFs and ARPE-19 cells
474 were used. For determination of relative epithelial cell infectivity viral stock dilutions
475 generating 300-1,500 RLUs in ARPE-19 cells were used.
476
477 **Fibroblast infection efficiency**
478 HFFs were seeded in white, clear, flat-bottom 96-well plates (Corning, Corning, New York) at
479 a density of 1 x 10^4 cells/well. The following day, viral stocks were diluted to similar number
480 of encapsidated genomes (range: 8.2 to 9.2 $\log_{10}$ genome copies/ml) in cell culture medium as
481 previously determined and 100 µl of viral dilution per well were used to infect the cells in

triplicates for 2 h at 37 °C. Cells were washed three times with PBS, supplied with 100 µl of medium and incubated further at 37 °C for 2 days before monitoring mean RLUs of technical triplicates. In parallel, 5 µl of the viral dilution was used to determine the actual number of encapsidated genomes used for infection. The ratio of $\log_{10}$ RLUs to $\log_{10}$ encapsidated genomes of parental strain was set at 1.0 and the fold change of the mutants as compared to parental strain was calculated. Three to four independent experiments per mutant were performed.

Relative epithelial cell infectivity

The same viral stock dilution was used for infection of both fibroblasts and epithelial cells each seeded in white, clear, flat-bottom 96-well plates at a density of 1 x 10^4 cells/well one day before infection. Two days after infection, RLUs were determined by luciferase assay as mentioned above and the epithelial to fibroblast RLU ratio was calculated. All experiments were performed in technical triplicates and three to four independent experiments were performed.

Production of purified virions for immunoblotting

Supernatants from infected HFFs were harvested when cells displayed > 90% CPE and then clarified by centrifugation at 4,000 x *g* for 30 min at 4 °C. After filtration through a 0.45 µm filter (Whatman, GE Healthcare Life Sciences, Thermo Fisher) viruses were concentrated by centrifugation at 4 °C using vivaspin 20 concentrators with a molecular weight cutoff of 100K (Sartorius, Göttingen, Germany). Thereafter, virions were purified by ultracentrifugation through a 20% sucrose TAN (0.05 M triethanolamine, 0.1 M NaCl, pH 8.0) cushion for 80 min at 70,000 x *g* at 4 °C and the pellets were gently resuspended in TAN buffer on ice and stored in aliquots at -80 °C until further use.

508 **Western blot analysis**

509 For sample preparation, virus stocks were mixed undiluted or diluted in TAN buffer with an
510 equal volume of reducing 2x sample buffer (125 mM Tris/Cl pH 6.8, 6% SDS, 10% glycerol,
511 10% 2-mercaptoethanol, 0.01% bromophenolblue) and incubated on ice for 10 min before
512 boiling at 95 °C for 10 min. Samples were separated on 10% SDS PAGE gels together with a
513 high-range rainbow marker (Amersham ECL High-Range Rainbow Molecular Weight Marker,
514 GE Healthcare, UK). Separated proteins were transferred to polyvinylidene difluoride (PVDF)
515 membranes (Immun-Blot, Bio-Rad, California, USA) in blotting buffer (40 mM Tris, 39 mM
516 glycine, 1.3 mM SDS, 20% methanol), which were then incubated overnight in blocking buffer
517 (PBS, 1% BSA, 0.1% Tween-20) at 4 °C. All antibodies (Abs) were diluted in blocking buffer.
518 Primary mouse anti-gH (AP86-SA4) and anti-MCP monoclonal antibodies (mAbs), anti-gO.02
519 mAb, and gB antibody (2F12; Abcam, Cambridge, UK) were incubated for 2 h at RT. Sheep,
520 anti-mouse IgG-HRP (Amersham, GE Healthcare, UK) was used as secondary antibody and
521 incubated for 1 h at RT. SuperSignal West Femto Maximum Sensitivity substrate (Thermo
522 Fisher) was applied for gO detection according to the manufacturer's instructions and Pierce
523 ECL Western Blotting Substrate (Thermo Fisher) for gH, MCP, and gB detection.
524 Chemiluminescent signals were visualized and analyzed using the ChemiDoc Imager and the
525 Image Lab 6.0 software (both Bio-Rad).

526

527 **Inhibition assays**

528 Cells were seeded in white, clear, flat-bottom 96-well plates at a density of 1 x 10^4 cells/well
529 the day before infection. A fixed amount of virus as determined by RLU normalization was pre-
530 incubated with serial dilutions of soluble forms of PDGFRα-Fc or NRP2-Fc, respectively, for
531 2 hours before infection. Two hours after infection cells were washed twice with 1x PBS,
532 supplied with 100 µl medium per well and further incubated for 2 days before subjected to
533 luciferase assay. Total RLUs and percentage relative to RLUs of mock-preincubated controls

were calculated. Two to five independent experiments per mutant viruses were performed and all experiments were carried out in technical triplicates. Another independently reconstituted BAC-derived virus per mutant was used to confirm the results.

Statistical analyses:

To compare relative epithelial cell infectivity (Figure 2) and percentage of infection after pre-treatment with soluble entry inhibitors, sPDGFRα and sNRP2, respectively, (Figures 4 and 5) between gO GT1c and gO GT mutants one-way ANOVA and Tukey' tests for multiple comparison were used. Mean RLU values from three to five independently repeated experiments were used for statistical analyses. P values < 0.05 were considered significant. GraphPad Prism version 7.01 was used for statistical analyses.

Acknowledgements

We are very grateful to Michaela Binder, Sylvia Malik, Barbara Dalmatiner, and Andreas Rohorzka for excellent technical support. We thank Nikolaus Osterrieder for generously providing the plasmid pEP-Kan-S for BAC mutagenesis.

Funding for this research was provided by a grant from the Austrian Science Fund (FWF) to I.G. (project number: P26420-B13). The funders had no role in study design, data collection and interpretation, or the decision to submit the work for publication.

Additional Information

Supplementary Information is provided.

References

1. Britt SBBaWJ. 2013. Synopsis of Clinical Aspects of Human Cytomegalovirus Disease. *In* Reddehase MJ (ed), Cytomegaloviruses: From Molecular Pathogenesis to Intervention, vol 1. Caister Academic Press.
2. Cannon MJ, Schmid DS, Hyde TB. 2010. Review of cytomegalovirus seroprevalence and demographic characteristics associated with infection. Rev Med Virol 20:202-13.
3. Sinzger C, Digel M, Jahn G. 2008. Cytomegalovirus cell tropism. Current topics in microbiology and immunology 325:63-83.
4. Huber MT, Compton T. 1998. The human cytomegalovirus UL74 gene encodes the third component of the glycoprotein H-glycoprotein L-containing envelope complex. Journal of virology 72:8191-7.
5. Wang D, Shenk T. 2005. Human cytomegalovirus virion protein complex required for epithelial and endothelial cell tropism. Proceedings of the National Academy of Sciences of the United States of America 102:18153-8.
6. Wang D, Shenk T. 2005. Human cytomegalovirus UL131 open reading frame is required for epithelial cell tropism. Journal of virology 79:10330-8.
7. Ciferri C, Chandramouli S, Donnarumma D, Nikitin PA, Cianfrocco MA, Gerrein R, Feire AL, Barnett SW, Lilja AE, Rappuoli R, Norais N, Settembre EC, Carfi A. 2015. Structural and biochemical studies of HCMV gH/gL/gO and Pentamer reveal mutually exclusive cell entry complexes. Proceedings of the National Academy of Sciences of the United States of America 112:1767-72.
8. Zhou M, Lanchy JM, Ryckman BJ. 2015. Human Cytomegalovirus gH/gL/gO Promotes the Fusion Step of Entry into All Cell Types, whereas gH/gL/UL128-131 Broadens Virus Tropism through a Distinct Mechanism. Journal of virology 89:8999-9009.

583 9. Jiang XJ, Adler B, Sampaio KL, Digel M, Jahn G, Ettischer N, Stierhof YD, Scrivano
584 L, Koszinowski U, Mach M, Sinzger C. 2008. UL74 of human cytomegalovirus
585 contributes to virus release by promoting secondary envelopment of virions. J Virol
586 82:2802-12.
587 10. Wille PT, Knoche AJ, Nelson JA, Jarvis MA, Johnson DC. 2010. A human
588 cytomegalovirus gO-null mutant fails to incorporate gH/gL into the virion envelope and
589 is unable to enter fibroblasts and epithelial and endothelial cells. Journal of virology
590 84:2585-96.
591 11. Zhou M, Yu Q, Wechsler A, Ryckman BJ. 2013. Comparative analysis of gO isoforms
592 reveals that strains of human cytomegalovirus differ in the ratio of gH/gL/gO and
593 gH/gL/UL128-131 in the virion envelope. Journal of virology 87:9680-90.
594 12. Murrell I, Tomasec P, Wilkie GS, Dargan DJ, Davison AJ, Stanton RJ. 2013. Impact of
595 sequence variation in the UL128 locus on production of human cytomegalovirus in
596 fibroblast and epithelial cells. Journal of virology 87:10489-500.
597 13. Zhang L, Zhou M, Stanton R, Kamil J, Ryckman BJ. 2018. Expression Levels of
598 Glycoprotein O (gO) Vary between Strains of Human Cytomegalovirus, Influencing the
599 Assembly of gH/gL Complexes and Virion Infectivity. Journal of virology 92.
600 14. Nguyen CC, Kamil JP. 2018. Pathogen at the Gates: Human Cytomegalovirus Entry
601 and Cell Tropism. Viruses 10.
602 15. Dolan A, Cunningham C, Hector RD, Hassan-Walker AF, Lee L, Addison C, Dargan
603 DJ, McGeoch DJ, Gatherer D, Emery VC, Griffiths PD, Sinzger C, McSharry BP,
604 Wilkinson GW, Davison AJ. 2004. Genetic content of wild-type human
605 cytomegalovirus. J Gen Virol 85:1301-12.
606 16. Sijmons S, Thys K, Mbong Ngwese M, Van Damme E, Dvorak J, Van Loock M, Li G,
607 Tachezy R, Busson L, Aerssens J, Van Ranst M, Maes P. 2015. High-throughput
608 analysis of human cytomegalovirus genome diversity highlights the widespread

609 occurrence of gene-disrupting mutations and pervasive recombination. Journal of
610 virology.
611 17. Suarez NM, Wilkie GS, Hage E, Camiolo S, Holton M, Hughes J, Maabar M, Vattipally
612 SB, Dhingra A, Gompels UA, Wilkinson GWG, Baldanti F, Furione M, Lilleri D,
613 Arossa A, Ganzenmueller T, Gerna G, Hubacek P, Schulz TF, Wolf D, Zavattoni M,
614 Davison AJ. 2019. Human Cytomegalovirus Genomes Sequenced Directly From
615 Clinical Material: Variation, Multiple-Strain Infection, Recombination, and Gene Loss.
616 The Journal of infectious diseases 220:781-791.
617 18. Mattick C, Dewin D, Polley S, Sevilla-Reyes E, Pignatelli S, Rawlinson W, Wilkinson
618 G, Dal Monte P, Gompels UA. 2004. Linkage of human cytomegalovirus glycoprotein
619 gO variant groups identified from worldwide clinical isolates with gN genotypes,
620 implications for disease associations and evidence for N-terminal sites of positive
621 selection. Virology 318:582-97.
622 19. Stanton R, Westmoreland D, Fox JD, Davison AJ, Wilkinson GW. 2005. Stability of
623 human cytomegalovirus genotypes in persistently infected renal transplant recipients. J
624 Med Virol 75:42-6.
625 20. Cudini J, Roy S, Houldcroft CJ, Bryant JM, Depledge DP, Tutill H, Veys P, Williams
626 R, Worth AJJ, Tamuri AU, Goldstein RA, Breuer J. 2019. Human cytomegalovirus
627 haplotype reconstruction reveals high diversity due to superinfection and evidence of
628 within-host recombination. Proceedings of the National Academy of Sciences of the
629 United States of America 116:5693-5698.
630 21. Lassalle F, Depledge DP, Reeves MB, Brown AC, Christiansen MT, Tutill HJ, Williams
631 RJ, Einer-Jensen K, Holdstock J, Atkinson C, Brown JR, van Loenen FB, Clark DA,
632 Griffiths PD, Verjans G, Schutten M, Milne RSB, Balloux F, Breuer J. 2016. Islands of
633 linkage in an ocean of pervasive recombination reveals two-speed evolution of human
634 cytomegalovirus genomes. Virus evolution 2:vew017.

635 22. Yan H, Koyano S, Inami Y, Yamamoto Y, Suzutani T, Mizuguchi M, Ushijima H,
636 Kurane I, Inoue N. 2008. Genetic linkage among human cytomegalovirus glycoprotein
637 N (gN) and gO genes, with evidence for recombination from congenitally and post-
638 natally infected Japanese infants. J Gen Virol 89:2275-9.
639 23. Kalser J, Adler B, Mach M, Kropff B, Puchhammer-Stockl E, Gorzer I. 2017.
640 Differences in Growth Properties among Two Human Cytomegalovirus Glycoprotein
641 O Genotypes. Frontiers in microbiology 8:1609.
642 24. Cui X, Freed DC, Wang D, Qiu P, Li F, Fu TM, Kauvar LM, McVoy MA. 2017. Impact
643 of Antibodies and Strain Polymorphisms on Cytomegalovirus Entry and Spread in
644 Fibroblasts and Epithelial Cells. Journal of virology 91.
645 25. Kabanova A, Marcandalli J, Zhou T, Bianchi S, Baxa U, Tsybovsky Y, Lilleri D,
646 Silacci-Fregni C, Foglierini M, Fernandez-Rodriguez BM, Druz A, Zhang B, Geiger R,
647 Pagani M, Sallusto F, Kwong PD, Corti D, Lanzavecchia A, Perez L. 2016. Platelet-
648 derived growth factor-alpha receptor is the cellular receptor for human cytomegalovirus
649 gHgLgO trimer. Nature microbiology 1:16082.
650 26. Stegmann C, Hochdorfer D, Lieber D, Subramanian N, Stohr D, Laib Sampaio K,
651 Sinzger C. 2017. A derivative of platelet-derived growth factor receptor alpha binds to
652 the trimer of human cytomegalovirus and inhibits entry into fibroblasts and endothelial
653 cells. PLoS pathogens 13:e1006273.
654 27. Wu Y, Prager A, Boos S, Resch M, Brizic I, Mach M, Wildner S, Scrivano L, Adler B.
655 2017. Human cytomegalovirus glycoprotein complex gH/gL/gO uses PDGFR-alpha as
656 a key for entry. PLoS pathogens 13:e1006281.
657 28. Wu K, Oberstein A, Wang W, Shenk T. 2018. Role of PDGF receptor-alpha during
658 human cytomegalovirus entry into fibroblasts. Proceedings of the National Academy of
659 Sciences of the United States of America 115:E9889-E9898.

660 29. Martinez-Martin N, Marcandalli J, Huang CS, Arthur CP, Perotti M, Foglierini M, Ho
661 H, Dosey AM, Shriver S, Payandeh J, Leitner A, Lanzavecchia A, Perez L, Ciferri C.
662 2018. An Unbiased Screen for Human Cytomegalovirus Identifies Neuropilin-2 as a
663 Central Viral Receptor. Cell 174:1158-1171 e19.
664 30. Stegmann C, Abdellatif ME, Laib Sampaio K, Walther P, Sinzger C. 2016. Importance
665 of highly conserved peptide sites of HCMV gO for the formation of the gH/gL/gO
666 complex. Journal of virology.
667 31. Stegmann C, Rothemund F, Laib Sampaio K, Adler B, Sinzger C. 2019. The N
668 Terminus of Human Cytomegalovirus Glycoprotein O Is Important for Binding to the
669 Cellular Receptor PDGFRalpha. Journal of virology 93.
670 32. Laib Sampaio K, Stegmann C, Brizic I, Adler B, Stanton RJ, Sinzger C. 2016. The
671 contribution of pUL74 to growth of human cytomegalovirus is masked in the presence
672 of RL13 and UL128 expression. The Journal of general virology 97:1917-27.
673 33. Hill AV. 1910. A new mathematical treatment of changes of ionic concentration in
674 muscle and nerve under the action of electric currents, with a theory as to their mode of
675 excitation. The Journal of physiology 40:190-224.
676 34. Li G, Nguyen CC, Ryckman BJ, Britt WJ, Kamil JP. 2015. A viral regulator of
677 glycoprotein complexes contributes to human cytomegalovirus cell tropism.
678 Proceedings of the National Academy of Sciences of the United States of America
679 112:4471-6.
680 35. Nguyen CC, Siddiquey MNA, Zhang H, Li G, Kamil JP. 2018. Human
681 Cytomegalovirus Tropism Modulator UL148 Interacts with SEL1L, a Cellular Factor
682 That Governs Endoplasmic Reticulum-Associated Degradation of the Viral Envelope
683 Glycoprotein gO. Journal of virology 92.

684 36. Puchhammer-Stöckl E, Görzer I. 2011. Human cytomegalovirus: an enormous variety
685 of strains and their possible clinical significance in the human host. Future Virology
686 6:259-271.
687 37. Görzer I, Kerschner H, Redlberger-Fritz M, Puchhammer-Stöckl E. 2010. Human
688 cytomegalovirus (HCMV) genotype populations in immunocompetent individuals
689 during primary HCMV infection. J Clin Virol 48:100-3.
690 38. Scrivano L, Sinzger C, Nitschko H, Koszinowski UH, Adler B. 2011. HCMV spread
691 and cell tropism are determined by distinct virus populations. PLoS pathogens
692 7:e1001256.
693 39. Tischer BK, Smith GA, Osterrieder N. 2010. En passant mutagenesis: a two step
694 markerless red recombination system. Methods in molecular biology 634:421-30.
695 40. Scrivano L, Sinzger C, Nitschko H, Koszinowski UH, Adler B. 2011. HCMV spread
696 and cell tropism are determined by distinct virus populations. PLoS Pathog 7:e1001256.

697

698

699

Tables

Table 1. Glycoprotein O and H content in fibroblast-derived cell-free virions.

Name of gO GT mutants	Envelope glycoproteins	
	gO in % [mean (range)]*	gH in % [mean (range)]*
GT1c	100	100
GT2b	not detectable	53 (14 - 92)
GT3	18 (8 - 28)	160 (142 - 178)
GT3/1c	6 (4 - 7)	not determined
GT1c/3	48 (46 - 50)	317 (208 - 425)
GT4	100 (83 - 116)	65 (50 - 80)
GT5	67 (53 - 80)	70 (40 - 100)

*) normalized to envelope glycoprotein B

Table 2. Dose-inhibition curve characteristics of gO genotype mutant strains.

Name of gO GT mutants	sPDGFRα-Fc dose-response curves in HFFs		sPDGFRα-Fc dose-response curves in ARPE-19 cells		sNRP2-Fc dose-response curves in ARPE-19 cells	
	IC_{50} in ng/ml [mean (range)]	slope (range)	IC_{50} in ng/ml [mean (range)]	slope (range)	IC_{50} in ng/ml [mean (range)]	slope (range)
GT1c	58 (52 - 63)	6.0 - 8.0	39 (16 - 53)	2.6 - 6.0	31 (18 - 44)	0.9 - 1.1
GT2b	73 (54 - 92)	6.0 - 8.0	36 (10 - 51)	2.6 - 3.0	65 (22 - 110)	1.2 - 1.5
GT3	65 (53 - 82)	4.8 - 10.0	47 (43 - 50)	4.7 - 6.0	34 (27 - 40)	1.1 - 1.5
GT3/1c	49 (46 - 54)	6.0 - 9.5	50 (49 - 50)	6.8 - 7.4	80 (50 - 110)	0.9 - 2.1
GT1c/3	69 (56 - 81)	2.5 - 6.2	30 (13 - 62)	1.0 - 2.6	65 (34 - 100)	0.9 - 1.3
GT4	52 (47 - 55)	5.5 - 6.0	55 (52 - 56)	5.3 - 6.0	90 (60 - 110)	0.7 - 1.3
GT5	68 (45 - 100)	5.3 - 8.0	56 (54 - 58)	5.3 - 6.0	67 (24 - 110)	1.2 - 1.7

The data shown are the results of two to five independent experiments. IC_{50} and slope values were calculated from [inhibitor] vs. response four-parameter dose-response curves.

Supplementary Table

Supplementary Table 1. Primer sequences for en passant mutagenesis

TB40-BAC4-luc-derived gO GT mutants	Template for PCR	PCR product	Forward primer (5' – 3')	Reverse primer (5' – 3')	BAC-DNA for recombination in GS1783
ΔgO	pEPKan-S	Recombination cassette	CAGAACTTTACTGCAACCACCACCAAAGG CTATTGAGGTTCCCCATGACAGAGGAGGA ATAGGGATAACAGGGTAATCGATTT	GCAGACGGACGGTGCGGGGTTTCCTCCT CTGTCATGGGGAACCCTCAATAGCCTTTG GTGGCCAGTGTTACAACCAATTAACC	TB40-BAC4-luc
GT2b	pEPKan-S	Insert for cloning into pEX-A258-Pgt2b	TAAGGAGCTCATGTTGAGAGTACCGTAAA TAGTGTACGGTGTTTCGTTACGGATCTAGG GATAACAGGGTAATCGATTT	GCCAGTGTTACAACCAATTAA	
	Transferplasmid	Recombination cassette	GATGGGAGCCTTTTGTATCGTA	GCCAAACCACAAGGCAGA	TB40-BAC4-lucΔgO
GT5	pEPKan-S	Insert for cloning into pEX-K4-Pgt5	TAAGGAGCTCATGTCAAGAGTGCCATAAA TAGTGTACGGCGTTTCGTTACGAATCTAGG GATAACAGGGTAATCGATTT	TAGCGAGCTCGCCAGTGTTACAACCAATT AACC	
	Transferplasmid	Recombination cassette	GGAGCCTTTTGTATCGTACTACGACATTGC TGCTTTCAGAACTTTACTGCGACCACCACC AAAGGCTATTG	AAACCACAAGGCAGACGGACGGTGCGG GGTTTCCTCCTCTGTCATGGGGAAAAAAG AGATGATAATGGTGAAAGGC	TB40-BAC4-lucΔgO
GT3; GT3/1c; GT1c/3	pEPKan-S	Insert for cloning into pEX-K4-Pgt3	TAAGGAGCTCATGTCAAGAGTGCCGTAAA TAGTGTACGGTGTTTCGTTGCGAATCTAGG GATAACAGGGTAATCGATTT	TAGCGAGCTCGCCAGTGTTACAACCAATT AACC	
	Transferplasmid	Recombination cassette	TTGCTGCTTTCAGAACTTTACTGCAACCAC CACCAAAGGCTATTGAGGGTAGACAGATT TACAGCCCGGC	CAAGGCAGACGGACGGTGCGGGGTTTCC TCCTCTGTCATGGGGAGAAAAGGAGAGAT GAGAGGTGTTTTTAACTTAT	TB40-BAC4-luc in GS1783

Figures

Figure 1.

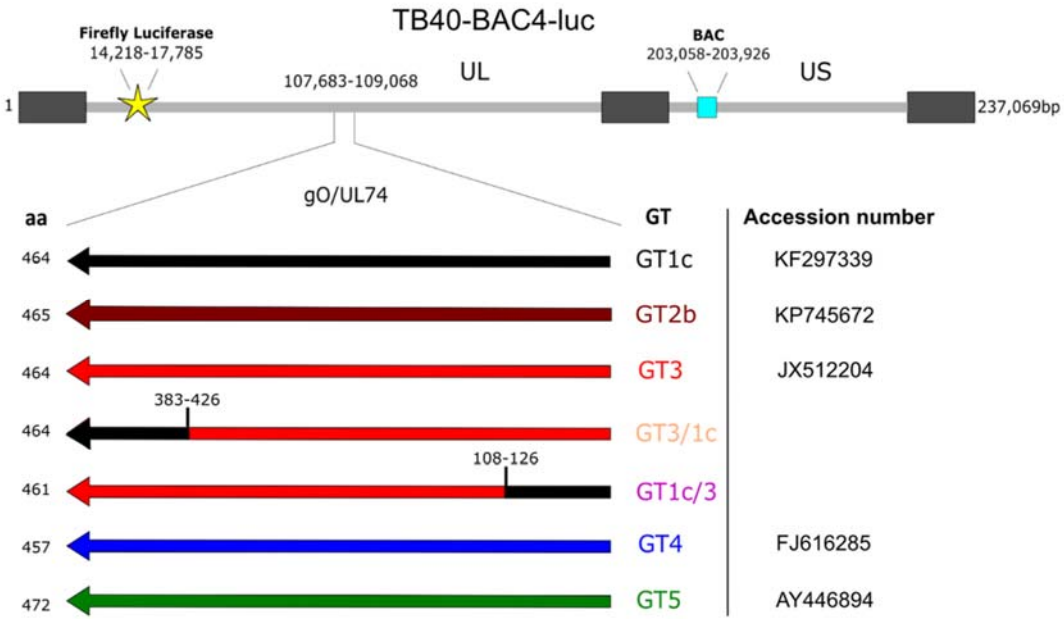

Figure 1. Schematic illustration of BAC-derived gO genotype mutants. The resident gO genotype (GT) 1c sequence of parental strain TB40-BAC4-luc was fully or partially replaced by the indicated gO GT sequences via „en passant“ mutagenesis. Main genome characteristics are displayed. Arrows represent orientation and position of gO ORFs upon GT swapping. GTs and accession numbers of the HCMV strains from which the respective gO GT sequences are derived are shown on the right and the length of gO amino acid (aa) sequence on the left. Aa range of the recombination breakpoint of the chimeric mutants GT3/1c and GT1c/3 are depicted above the ORF. Cell-free bacterial artificial chromosome-derived mutant virus stocks were generated upon reconstitution in human foreskin fibroblasts.

Figure 2.

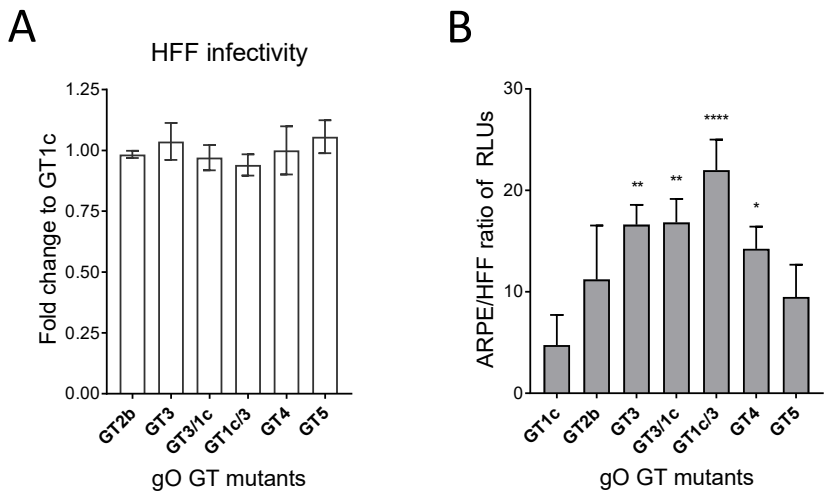

Figure 2. Cell-free infectivity of gO genotype mutants for fibroblasts and epithelial cells. A) Human foreskin fibroblasts (HFFs) were infected with parental strain gO GT1c and the panel of gO GT mutants using similar numbers of encapsidated genome equivalents (range: 8.0 – 9.2 $\log_{10}$ copies/ml). Two days post infection relative light units (RLUs) were assessed in cell lysates by luciferase assay as a read out of infection efficiency. Log_{10} RLU to genome ratio was calculated and the fold change relative to gO GT1c was determined. All experiments were performed in triplicates and data shown are means ± SEM of 2 - 4 independent experiments. B) HFFs and ARPE-19 cells were simultaneously infected with parental strain gO GT1c and the gO GT mutants using the same virus preparation for both cell types. Two days post infection RLUs were determined and the ratio of fibroblast to epithelial cell RLUs was calculated. All experiments were performed in triplicates and data shown are means ± SEM of 3 - 4 independent experiments. Statistical significance was evaluated by ANOVA with Tukey's test for multiple comparison. ****$p<0.0001$; **$p<0.01$; *$p<0.05$ in comparison to GT1c.

Figure 3.

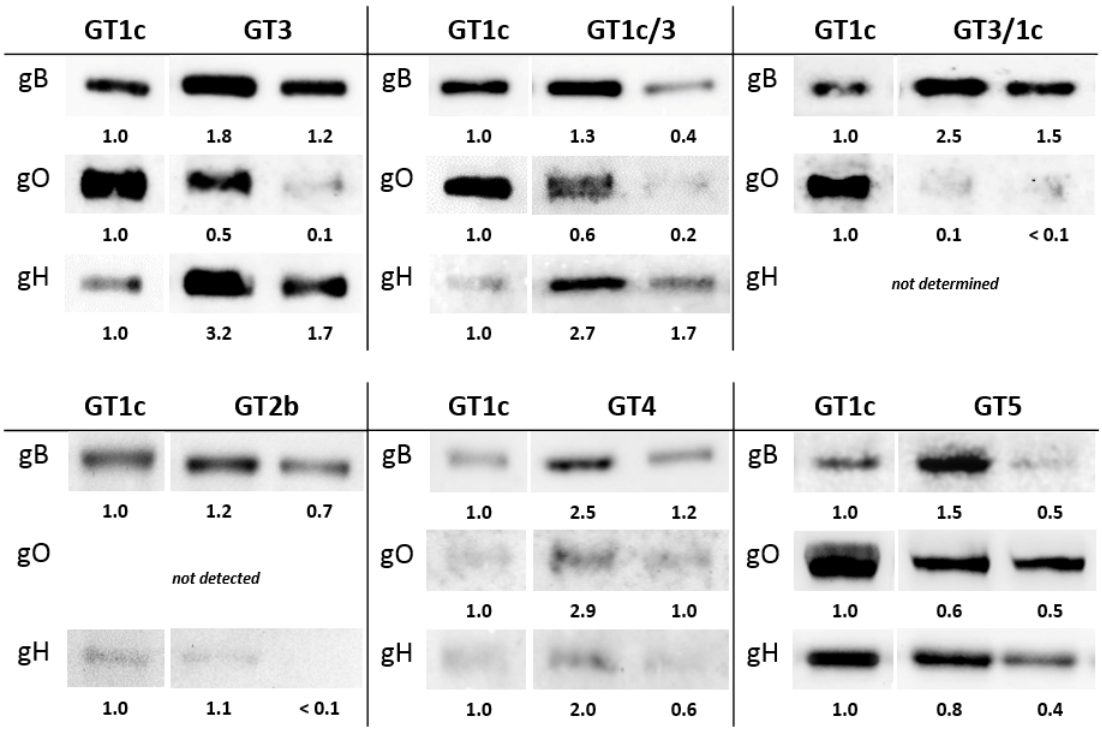

Figure 3. Comparison of gO and gH content in cell-free virions between parental strain gO GT1c and gO mutants. Virions harvested from human foreskin fibroblast supernatant were subjected to reducing gel electrophoresis and analyzed by Western Blot using antibodies directed against glycoproteins gB (anti-gB mAb 2F12), gO (anti-gO.02 mAb) and gH (AP86-SA4). The amount of virions loaded on the gels were compared to gB. Contents of gO and gH were compared between gO GT1c and the respective gO mutants. For each mutant an additional 2-fold dilution was loaded on the gel. Band densities were determined relative to the GT1c reference band for each blot individually, and are shown below the blots.

Figure 4.

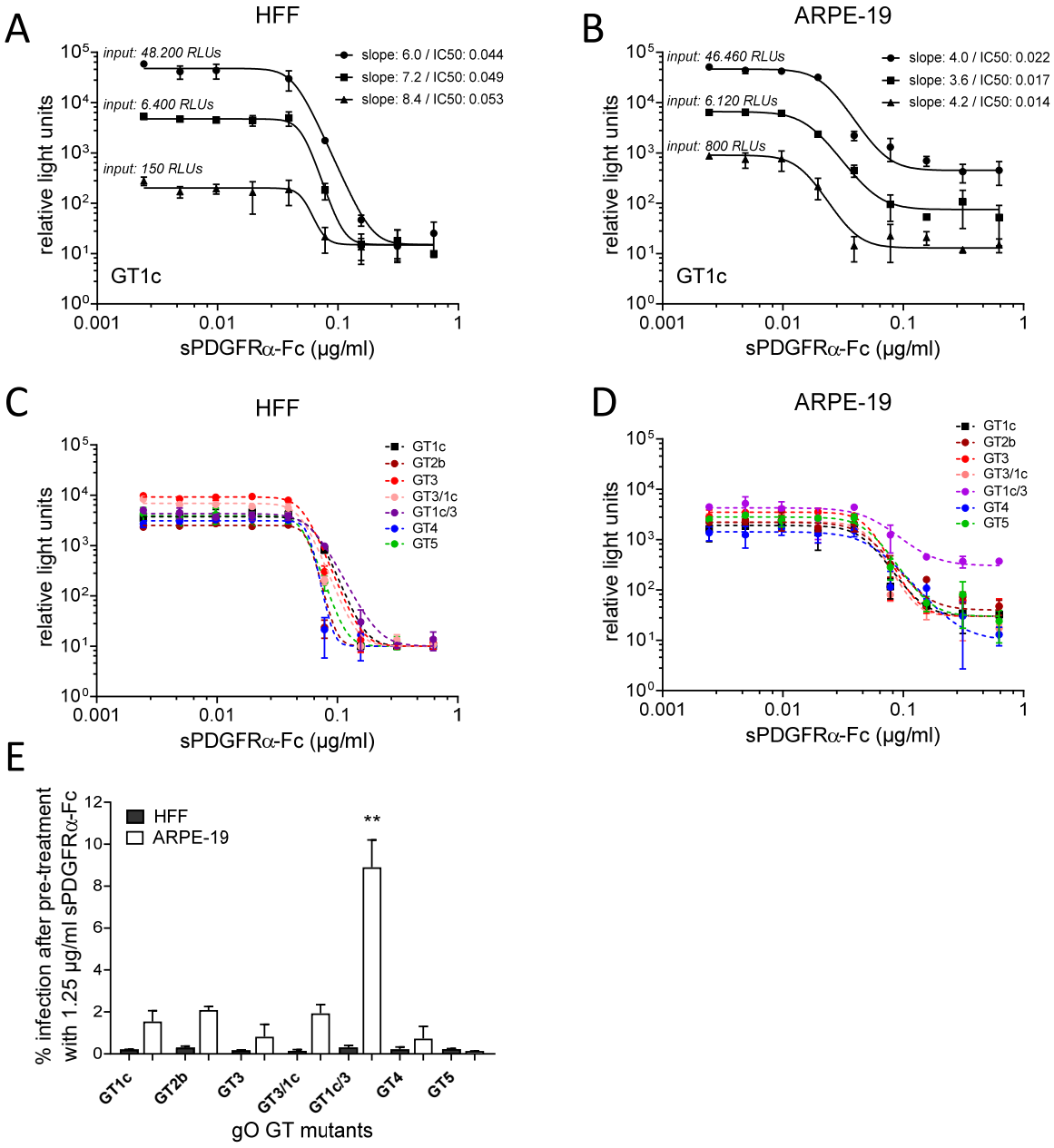

Figure 4. Inhibition of cell-free infectivity of gO genotype mutant viruses by soluble PDGFRα-Fc. The whole panel of gO genotype (GT) mutants along with parental strain gO GT1c were pre-incubated with soluble PDGFRalpha-Fc (sPDGFRα-Fc) before infection of human foreskin fibroblasts (HFFs) or adult retinal pigment epithelial cells 19 (ARPE-19 cells), respectively. Two days after infection relative light units (RLUs) were determined in cell lysates by a luciferase assay. In (A) and (B) three different virus stock concentrations of parental strain gO GT1c indicated as input RLUs are used. In (C to E) mutant

857 virus stocks were diluted to achieve RLUs ranging from 1.000 to 19.000 without treatment. In (A to D)
858 parental and mutant virus stocks were treated with serial 2-fold dilutions of sPDGFRα-Fc (range: 0.625
859 to 0.0244 µg/ml). Monitored RLUs were plotted against sPDGFRalpha-Fc concentrations. Four-
860 parameter dose-response curves were generated and the protein concentration causing inhibition of
861 50% of infection (IC50) and the steepness of the curves were calculated (see in A and B and in Table
862 1). In (C) and (D) one representative curve from each mutant out of 2 – 4 independent experiments is
863 shown. Data represent mean values ± SDs of triplicate determinations. In (E) the % of infection of HFFs
864 or ARPE-19 cells, respectively, after pre-treatment with 1.25µg/ml sPDGFRα-Fc is shown. Experiments
865 were performed in triplicates and data are means ± SEM of 3 - 5 independent experiments. Statistical
866 significance was evaluated by ANOVA with Tukey's test for multiple comparison. **$p<0.01$ in
867 comparison to GT1c.
868

Figure 5.

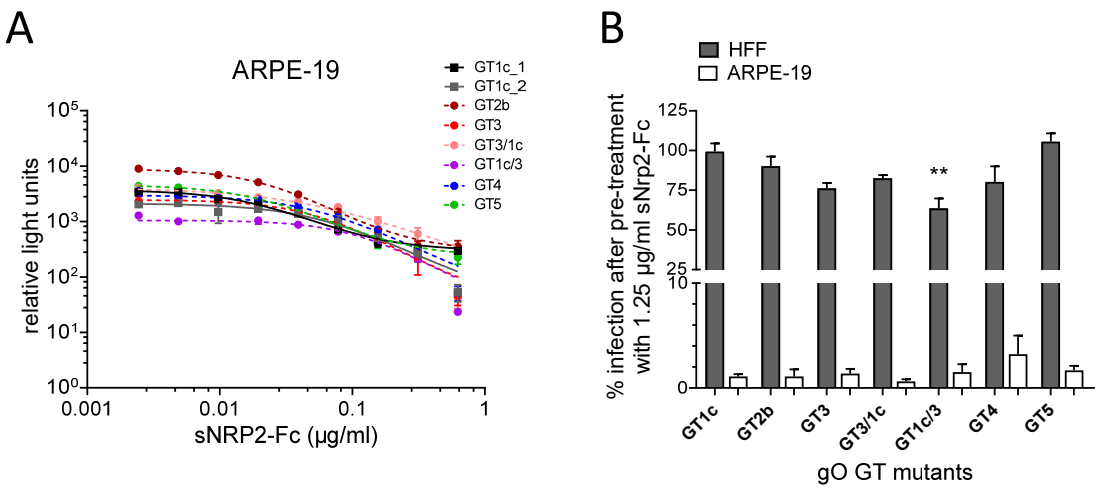

Figure 5. Inhibition of cell-free infectivity of gO genotype mutant viruses by soluble NRP2-Fc. A) Parental gO GT1c and gO GT mutant virus stocks were pre-incubated with serial 2-fold dilutions of soluble NRP2-Fc (sNRP2-Fc) (range: 0.625 to 0.0244 µg/ml) before infection of adult retinal pigment epithelial cells 19 (ARPE-19 cells). Two days after infection relative light units (RLUs) were monitored ranging from 1.000 to 10.000 RLUs in untreated controls. RLUs were plotted against sNRP2-Fc concentrations and four-parameter dose-response curves were generated to calculate the protein concentration causing inhibition of 50% of infection (IC50) and to determine the steepness of the curves. Two curves from gO GT1c and one representative curve from each mutant out of 2 independent experiments is shown. Virus stock concentrations used were similar as for (A). Data represent mean values ± SDs of triplicate determinations. B) The % of infection of HFFs or ARPE-19 cells, respectively, after pre-treatment with 1.25µg/ml sNRP2-Fc is shown. Experiments were performed in triplicates and data are means ± SEM of 3 - 5 independent experiments. Statistical significance was evaluated by ANOVA with Tukey's test for multiple comparison. **p<0.01 in comparison to GT1c.

Supplementary figures

Figure S1

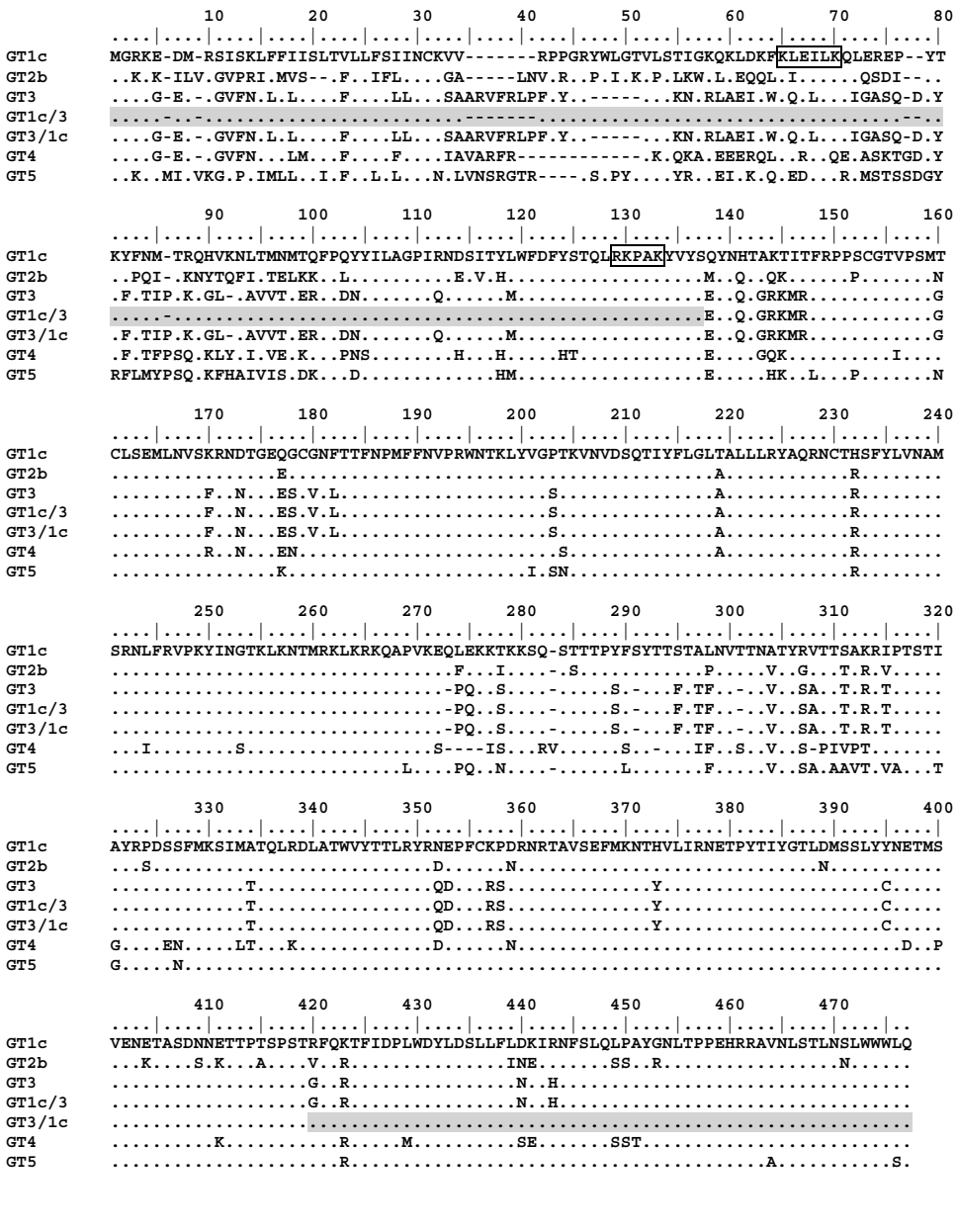

Supplementary Figure S1: Amino acid alignment of gO genotype mutant sequences. Reference sequence of genotype (GT) 1c (TB40-BAC4; ABV71596.1) is aligned with GT2b (BE/29/2011; AKI14139.1), GT3 (HAN16; AFR55727.1), GT4 (Towne, ACM48052.1), gO GT5 (Merlin, AAR31626.1), and the two recombinant forms, GT1c/3 and GT3/1c. Putative PDGFRalpha binding sites as characterized recently (Stegmann et al., 2019) are depicted by black boxes. The grey-shaded regions of recombinant GT1c/3 and GT3/1c mutants indicate the GT1c sequence part.

Figure S2

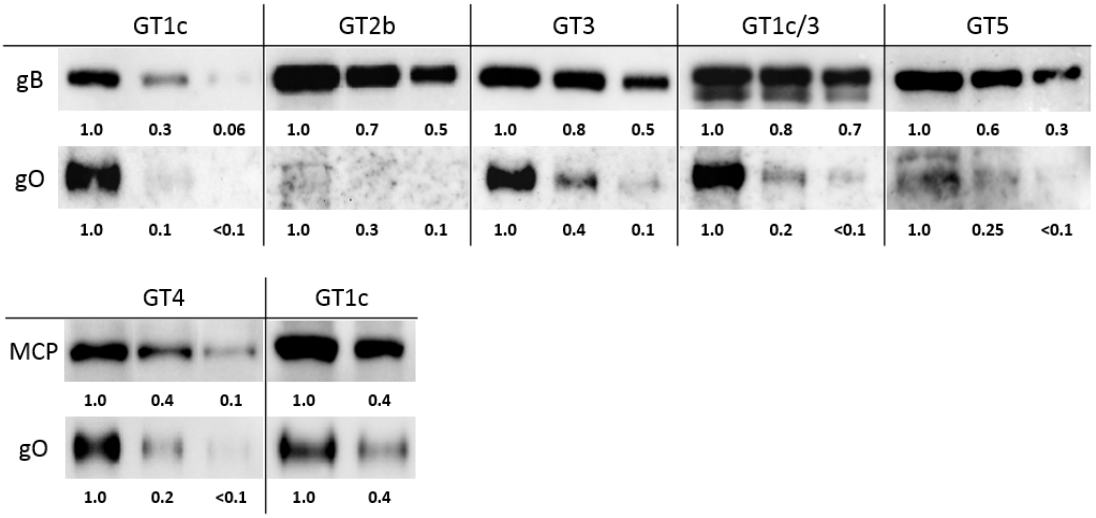

Supplementary Figure S2. Reactivity of monoclonal anti-gO antibody, anti-gO.02 mAb, against distinct gO genotypic forms. Two to three 2-fold dilutions of virions were loaded on the gels. Reactivity against gO was compared to reactivity directed against gB (anti-gB mAb 2F12) or major capsid protein (MCP).